Journal of Materials Chemistry C

PAPER

View Article Online
View Journal | View Issue

Cite this: J. Mater. Chem. C, 2018, 6, 11465

Novel $Al_2Mo_3O_{12}$-based temperature-stable microwave dielectric ceramics for LTCC applications†

Junqing Ren,[ab] Ke Bi,[a] Xiuli Fu*[a] and Zhijian Peng*[b]

Received 11th August 2018,
Accepted 28th September 2018

DOI: 10.1039/c8tc04014a

rsc.li/materials-c

Microwave dielectric ceramics are key materials in low-temperature co-fired ceramic (LTCC) technology. In many material systems, Mo-based microwave dielectric ceramics have attracted world-wide attention in recent years due to their low intrinsic sintering temperature and high quality factor ($Q \times f$). In combination with its low dielectric constant (ε_r), $Al_2Mo_3O_{12}$ is a very promising LTCC candidate, but the very negative temperature coefficient of its resonant frequency (τ_f) limits its application. In this work, novel $(1-x)Al_2Mo_3O_{12}$–$xTiO_2$ (x = 0–0.4) microwave dielectric ceramics were designed and prepared by a conventional solid-state reaction. The effects of TiO_2 addition on the phase composition, microstructure, and microwave dielectric properties of the obtained $Al_2Mo_3O_{12}$-based ceramics were investigated. It was revealed that rutile TiO_2 could co-exist with monoclinic $Al_2Mo_3O_{12}$ in the samples after they were prepared under optimized conditions. With increasing addition of TiO_2, the ε_r value of the obtained ceramics increased from 5.69 to 6.85, the value of $Q \times f$ decreased from 73 910 to 45 720 GHz, and τ_f varied from −32.3 to +9.2 ppm °C^{-1}. When x = 0.3, microwave dielectric ceramics of near-zero τ_f (ε_r = 6.23, $Q \times f$ = 51 630 GHz, and τ_f = −3.3 ppm °C^{-1}) could be obtained. Such high-performance microwave dielectric ceramics would be promising for LTCC applications.

1. Introduction

Next-generation wireless communication systems require a high frequency, miniaturization, and a low loss of the electronic devices and substrates. As the key technology involved in electronic packaging, low-temperature co-fired ceramics (LTCCs) enable the integration of electronic components in three-dimensional modularization and have widely been used in high-frequency communications.[1–5] Specifically, for the dielectric ceramics in LTCCs, a sintering temperature lower than the melting point of silver or other metal electrodes should be ensured. Furthermore, for high-performance applications of ceramic dielectric layers (substrates), a low dielectric constant (ε_r, generally lower than 10) could increase the speed of the signal transmission, a high quality factor ($Q \times f$, higher than at least 1000 GHz) can satisfy applications at higher frequencies, and a temperature coefficient of the resonant frequency (τ_f) close to zero would ensure the temperature stability of the devices.[1–3] Therefore, various microwave dielectric ceramics with low sintering temperatures and excellent performance have been extensively investigated.

In the literature, many ceramics with high intrinsic sintering temperatures were processed to reduce the sintering temperature by adding sintering aids, so as to accommodate LTCC applications.[6–8] However, such a method will introduce a number of second phases, which would seriously degrade the microwave dielectric properties of the obtained ceramics. Therefore, exploring microwave ceramic matrices with low intrinsic sintering temperatures and excellent performance has been a hot topic in this field. In particular, several low-cost and low-toxicity Mo-based dielectric ceramics have attracted much attention due to their low sintering temperatures (<950 °C) and good microwave dielectric properties.[9–14] For example, $Na_2Mo_2O_7$ ceramics sintered at 575 °C were reported to present microwave dielectric properties of $\varepsilon_r \sim 12.9$, $Q \times f \sim 62\,400$ GHz, and $\tau_f \sim -72$ ppm °C^{-1}.[15] $La_2Mo_3O_{12}$ sintered at 930 °C showed microwave dielectric properties of $\varepsilon_r \sim 10.1$, $Q \times f \sim 60\,000$ GHz, and $\tau_f \sim -80$ ppm °C^{-1}.[16]

However, in the last two decades, $Al_2Mo_3O_{12}$ has been widely studied just for its negative thermal expansion coefficient when it is used as a substrate.[17–21] As a potentially excellent substrate material in the field of microelectronics, it was not until 2011 that Surjith *et al.* first reported the microwave dielectric properties of $Al_2Mo_3O_{12}$ (ε_r = 6.4, $Q \times f$ = 49 225 GHz, and τ_f = −41 ppm °C^{-1}), which was sintered at 810 °C for 2 h.[22] Since the relative density of the reported $Al_2Mo_3O_{12}$ ceramics is only 85%,[22] the optimum

[a] State Key Laboratory of Information Photonics and Optical Communications, and School of Science, Beijing University of Posts and Telecommunications, Beijing 100876, P. R. China. E-mail: xiulifu@bupt.edu.cn
[b] School of Science, China University of Geosciences, Beijing 100083, P. R. China. E-mail: pengzhijian@cugb.edu.cn

† Electronic supplementary information (ESI) available. See DOI: 10.1039/c8tc04014a

sintering processes for $Al_2Mo_3O_{12}$ ceramics are certainly worth further exploring. Unfortunately, the large negative τ_f value limits their application in many devices that are sensitive to ambient temperatures.

In order to achieve dielectric ceramics with a near-zero τ_f, one of the effective methods is to add components with an opposite τ_f value to form a composite. For example, rutile TiO_2 has a large positive τ_f value (+460 ppm $^\circ C^{-1}$), which has successfully been used to compensate the negative τ_f value of many microwave dielectric ceramics.[23–26] What's more, in many Mo-based ceramics, TiO_2 will not react with the matrix to produce second phases that will degrade the quality factor.

Taking all these factors into account, in this work, in order to adjust the τ_f value of $Al_2Mo_3O_{12}$-based composite ceramics to near zero, novel $(1-x)Al_2Mo_3O_{12}$–$xTiO_2$ (x = 0, 0.1, 0.2, 0.3, and 0.4) systems were designed, which were simply fabricated by conventional solid-state reaction sintering. The effects of TiO_2 addition on the phase composition, microstructure, and microwave dielectric properties of the obtained $Al_2Mo_3O_{12}$-based ceramics were investigated. Surprisingly, at the optimized low sintering temperature of 790 °C for 12 h, optimal microwave dielectric ceramics ($0.7Al_2Mo_3O_{12}$–$0.3TiO_2$) of near-zero τ_f (−3.3 ppm $^\circ C^{-1}$) and excellent dielectric properties (ε_r = 6.23 and $Q \times f$ = 51 630 GHz) were obtained. Such high-performance microwave dielectric ceramics would be very promising LTCC candidates for microwave wireless communications.

2. Experimental

2.1 Sample preparation

The samples were prepared by using a conventional two-step solid-state reaction and sintering method. In the optimized processes (see Fig. S1–S13 in ESI†), analytical-grade Al_2O_3 and MoO_3 powders were first weighed according to the stoichiometry of $Al_2Mo_3O_{12}$. The powders were then mixed by ball-milling for 24 h with absolute ethanol as the dispersive media and highly resistant zirconia balls as the grinding media. After milling, the resultant slurry was dried at 100 °C for 24 h in an open oven. After drying, the composite powder was calcined at 750 °C for 4 h in a Muffle oven. After calcination, the powder chunks were crushed into a fine powder and re-milled with TiO_2 for 12 h, as done for the above Al_2O_3 and MoO_3 mixture *via* ball-milling, in which the samples were designed in a nominal composition of $(1-x)Al_2Mo_3O_{12}$–$xTiO_2$ (x = 0, 0.1, 0.2, 0.3, and 0.4). After drying again, the resultant powder chunks were ground with 5% PVA as a binder and sieved into a fine powder. Then, the obtained powder was pressed into cylinders (10 mm in diameter and 5 mm in height). All the green bodies were then sintered in a Muffle oven at 790 °C for 12 h, and cooled down naturally to room temperature.

2.2 Material characterization

Crystallographic analysis of the as-sintered samples was performed by an X-ray diffractometer (XRD, D/max-RB, Cu Kα, λ = 1.5418 Å). The scanning 2θ angle was in the range of 20°–50°, and the scanning rate was 6° min^{-1}. The lattice parameter was calculated from the XRD data by Jade 6 PC software, and the phase composition in the samples was calculated by the relative intensity ratio (RIR) method. The microstructure was examined by a scanning electron microscope (FE-SEM, S4800) on the fresh fractured surfaces of the samples. From the obtained SEM images, the grain size was evaluated using Nano Measurer 1.2 PC software. The displayed grain size for each sample was the mean value of all the grains identified from the whole image. The composition was measured using an energy dispersive X-ray spectroscope (EDX) attached to the SEM. The apparent density was measured by the Archimedes method according to the international standard ISO18754. The theoretical density of the obtained $(1-x)Al_2Mo_3O_{12}$–$xTiO_2$ ceramics was calculated by the mixture rule:

$$\rho = \frac{\rho_1 \times \nu_1 + \rho_2 \times \nu_2}{\nu_1 + \nu_2}, \quad (1)$$

where ρ_1 and ρ_2 are the theoretical densities of each phase, and ν_1 and ν_2 represent their volumes, respectively. The relative density of the samples was defined as the percentage of the apparent density to their corresponding theoretical density. The microwave dielectric properties were measured using the cavity method in $TE_{01\delta}$ mode (E5063A Vector Network Analyzer). In addition, the temperature coefficient of the resonant frequency (τ_f) was calculated by the following equation:

$$\tau_f = \frac{f_{t_2} - f_{t_1}}{f_{t_1}(t_2 - t_1)}, \quad (2)$$

where f_{t_1} and f_{t_2} are the resonant frequencies at the measuring temperatures t_1 (25 °C) and t_2 (85 °C), respectively.

3. Results and discussion

3.1 Composition and microstructure

Fig. 1 displays the XRD patterns of the obtained $(1-x)Al_2Mo_3O_{12}$–$xTiO_2$ (x = 0, 0.1, 0.2, 0.3, and 0.4) ceramics. It is known that $Al_2Mo_3O_{12}$ crystallizes into a monoclinic structure at room temperature and will present an orthorhombic structure after the transition temperature.[18,19] From the recorded XRD patterns,

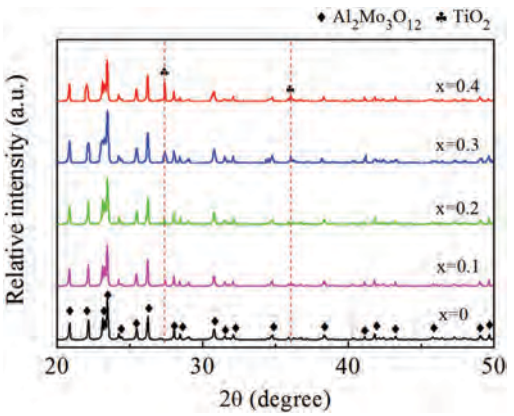

Fig. 1 XRD patterns of the obtained $(1-x)Al_2Mo_3O_{12}$–$xTiO_2$ (x = 0, 0.1, 0.2, 0.3, and 0.4) ceramics sintered at 790 °C for 12 h.

$Al_2Mo_3O_{12}$ with a monoclinic structure (JCPDS card no. 84-1652) could be identified. After adding TiO_2, rutile TiO_2 (JCPDS card no. 21-1276) could be detected, and the intensities of its diffraction peaks would increase with increasing addition of TiO_2, implying that rutile TiO_2 could coexist with monoclinic $Al_2Mo_3O_{12}$ in the obtained samples. Moreover, no other phases could be identified in any of the samples, indicating that both the rutile TiO_2 and monoclinic $Al_2Mo_3O_{12}$ phases are stable in the designed samples after they were prepared under the optimized conditions (specifically, sintering at 790 °C for 12 h). In addition, the cell volumes of the obtained $(1 - x)Al_2Mo_3O_{12}$–$xTiO_2$ (x = 0, 0.1, 0.2, 0.3 and 0.4) ceramics were calculated from the XRD data, which were 1987.27, 2042.99, 2145.85, 2001.82, and 2086.72 Å^3 for the samples with x = 0, 0.1, 0.2, 0.3, and 0.4, respectively. It is noted that the radius of the Ti^{4+} ions (0.605 Å) is larger than that of the Mo^{6+} (0.41 Å) and Al^{3+} (0.535 Å) ions. However, with an increase in the added amount of TiO_2, no monotonicity in the variation of the cell volumes could be observed, revealing that the substitution of Ti^{4+} ions for Mo^{6+} and Al^{3+} ions did not happen in the samples after the addition of TiO_2. All these results indicate that the obtained $(1 - x)Al_2Mo_3O_{12}$–$xTiO_2$ (x = 0, 0.1, 0.2, 0.3, and 0.4) ceramics are stable composites with the coexistence of rutile TiO_2 and monoclinic $Al_2Mo_3O_{12}$, which guarantees the high microwave dielectric performance of the obtained ceramics.

Typical SEM images of the obtained $(1 - x)Al_2Mo_3O_{12}$–$xTiO_2$ (x = 0, 0.1, 0.2, 0.3, and 0.4) ceramics are exhibited in Fig. 2. It is seen that dense microstructures can be observed for all the samples. However, the pure $Al_2Mo_3O_{12}$ ceramic sample exhibits a relatively inhomogeneous grain distribution with an average size of 6.09 μm. After adding TiO_2, the mean size of the $Al_2Mo_3O_{12}$ grains gradually decreases (see Fig. S14, ESI†). This result implies that the added TiO_2 could inhibit the growth of the $Al_2Mo_3O_{12}$ grains. Moreover, it can be seen from the images that there are two different types of grain in the TiO_2-added samples, which can be confirmed by EDX analysis (see Fig. S15, ESI†). The smaller ones are TiO_2 grains and the bigger ones are $Al_2Mo_3O_{12}$ grains. This result is consistent with the XRD

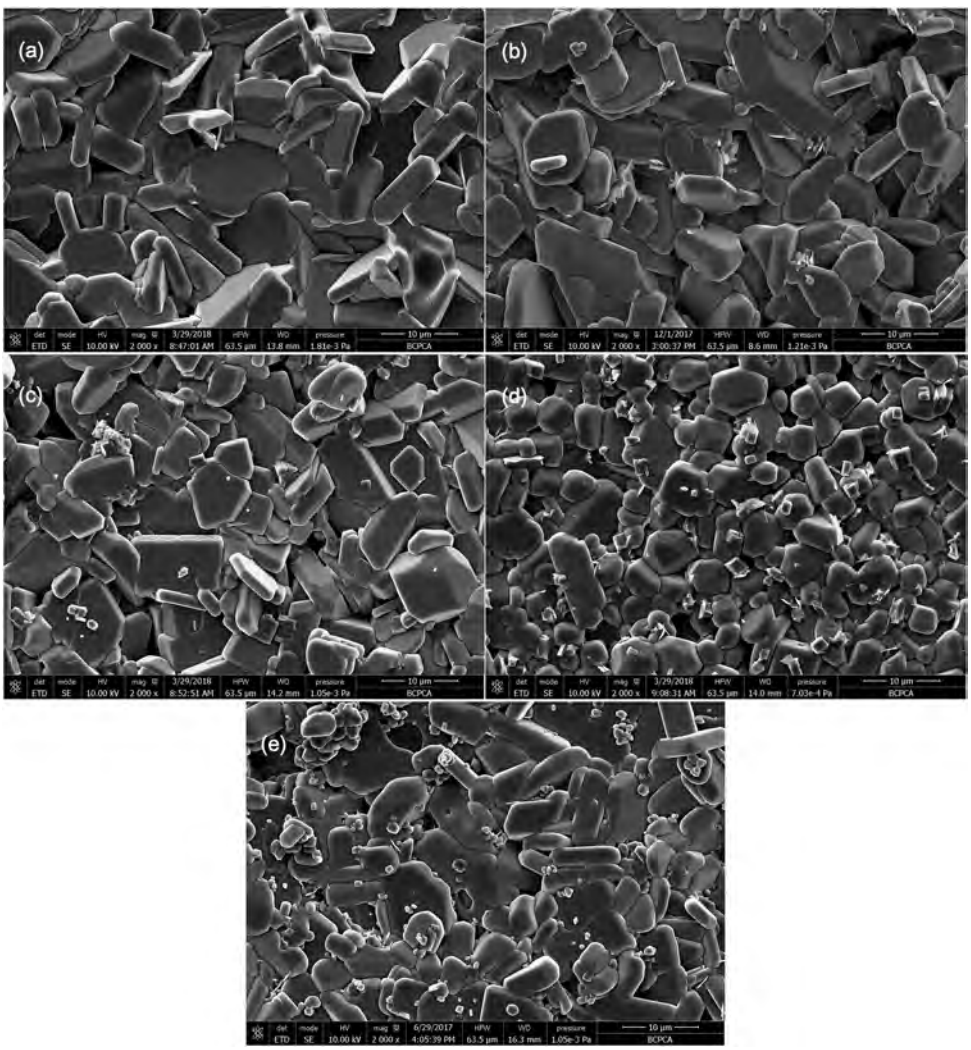

Fig. 2 Typical SEM images of the obtained $(1 - x)Al_2Mo_3O_{12}$–$xTiO_2$ ceramics sintered at 790 °C for 12 h with x = : (a) 0, (b) 0.1, (c) 0.2, (d) 0.3 and (e) 0.4. All the images were taken on the fracture surface of the samples.

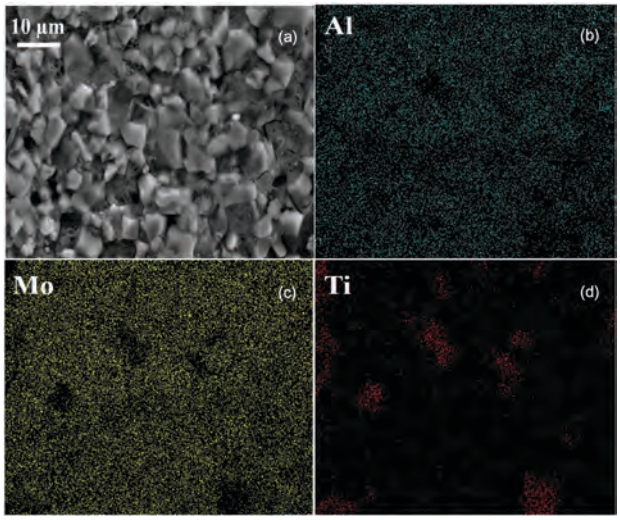

Fig. 3 EDX mapping results of the obtained $0.6Al_2Mo_3O_{12}$–$0.4TiO_2$ ceramic sample sintered at 790 °C for 12 h on a polished surface: (a) scanning area, and (b–d) EDX mapping spectra of Al, Mo, and Ti, respectively.

observations. The size of the TiO_2 grains is smaller than that of the $Al_2Mo_3O_{12}$ grains, possibly due to their much higher sintering temperature (about 1200 °C) than that of $Al_2Mo_3O_{12}$.[27,28] In order to further investigate the distribution of TiO_2, EDX mapping analysis of a typical $0.6Al_2Mo_3O_{12}$–$0.4TiO_2$ ceramic sample was carried out, and the results are presented in Fig. 3. It can be seen from this figure that the Al and Mo ions are distributed homogeneously over the sample, while the Ti ions are decorated among the samples. In combination with the SEM observations (see Fig. 2), it can concluded that TiO_2 is segregating into the boundary of the $Al_2Mo_3O_{12}$ grains. This result is also consistent with the XRD analysis.

3.2 Microwave dielectric properties

Fig. 4 presents the relative density and dielectric constant (ε_r) of the obtained $(1 - x)Al_2Mo_3O_{12}$–$xTiO_2$ ceramics sintered at 790 °C for 12 h as a function of the x value. The relative density almost remains constant over 95.5% when $0 \leq x \leq 0.2$, but with $x \geq 0.3$, it decreases slightly, reaching 94.8% when $x = 0.4$. These results indicate that the added TiO_2 grains hinder the sintering of the samples due to their high melting point. Meanwhile, the ε_r value continuously increases from 5.69 to 6.85 when the x value increases from 0 to 0.4. Generally speaking, ε_r is mainly determined by the ionic polarizabilities, second phases, and pores/density in microwave dielectric ceramics.[29–31] For the present $(1 - x)Al_2Mo_3O_{12}$–$xTiO_2$ composite system, the ε_r value would not be affected by the ionic polarizability because ion substitution did not occur. Thus, the increase in the ε_r value should be caused by the high ε_r value of TiO_2, because the slightly decreased relative density would contribute to a decrease of ε_r somewhat. Moreover, for a two-phase composite, the Lichtenecker empirical logarithmic rule is the common model to predict the ε_r value:[32,33]

$$\log \varepsilon_r = \nu_1 \log \varepsilon_1 + \nu_2 \log \varepsilon_2, \quad (3)$$

where ν_1 and ν_2 represent the volume fractions of the components (here, $Al_2Mo_3O_{12}$ and TiO_2), while ε_{r1} and ε_{r2} are their ε_r values, respectively. Based on this model, the theoretical ε_r values of the present $(1 - x)Al_2Mo_3O_{12}$–$xTiO_2$ composites are exhibited by the dashed line in Fig. 4. It can be seen from this figure that the measured ε_r value fits well with the theoretical one for the samples with $0 \leq x \leq 0.2$. However, when $x \geq 0.3$, the measured ε_r value is lower than the theoretical one, which should be attributed to the increased number of pores in such samples, which is consistent with the decrease in the relative density.

Fig. 5 illustrates the quality factor ($Q \times f$) of the obtained $(1 - x)Al_2Mo_3O_{12}$–$xTiO_2$ (x = 0, 0.1, 0.2, 0.3, and 0.4) ceramics. As can be seen in this figure, the $Q \times f$ value decreases from 73 910 to 45 720 GHz when the x value is increased from 0 to 0.4. It is known that the factors influencing the $Q \times f$ value of microwave ceramics not only include the intrinsic ones mainly contributing to the lattice vibration mode, but also the extrinsic ones, such as the second phases, grain morphology, and densification of the samples.[29,30] Here, the extrinsic factors play a major role in the change in the $Q \times f$ value of the obtained $(1 - x)Al_2Mo_3O_{12}$–$xTiO_2$ ceramics. The added second-phase TiO_2

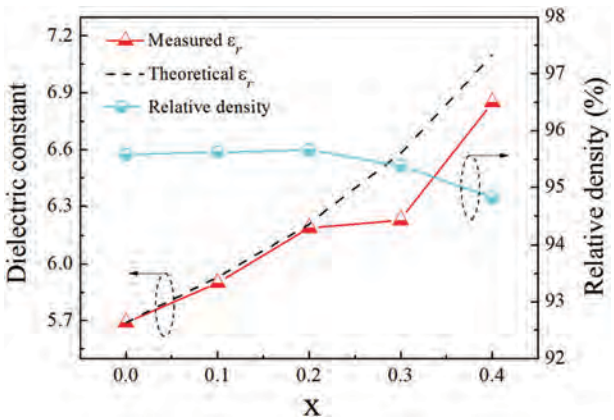

Fig. 4 Dielectric constant and relative density of the obtained $(1 - x)Al_2Mo_3O_{12}$–$xTiO_2$ (x = 0, 0.1, 0.2, 0.3, and 0.4) ceramics sintered at 790 °C for 12 h.

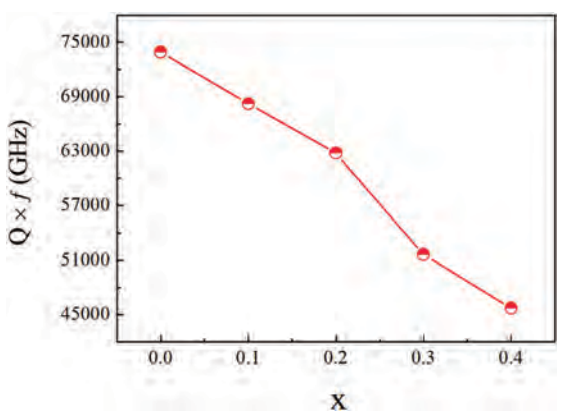

Fig. 5 Quality factor of the obtained $(1 - x)Al_2Mo_3O_{12}$–$xTiO_2$ (x = 0, 0.1, 0.2, 0.3, and 0.4) ceramics sintered at 790 °C for 12 h.

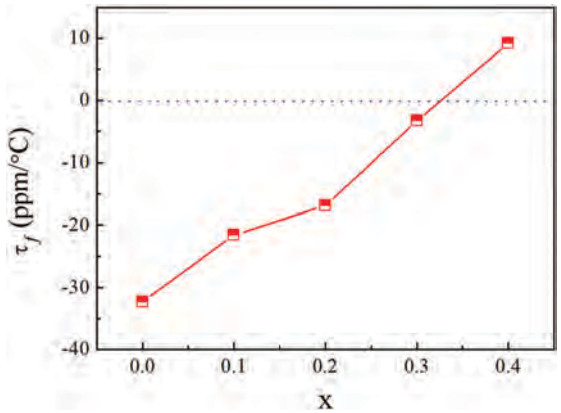

Fig. 6 Temperature coefficients of the resonant frequencies of the obtained $(1-x)Al_2Mo_3O_{12}$–$xTiO_2$ (x = 0, 0.1, 0.2, 0.3, and 0.4) ceramics sintered at 790 °C for 12 h.

has a lower $Q \times f$ value than $Al_2Mo_3O_{12}$, which would reduce the $Q \times f$ value of their composite ceramics continuously when x is increased from 0 to 0.4. What's more, after adding TiO_2, the increased number of grain boundaries caused by the reduction in mean grain size would also decrease the $Q \times f$ value of the obtained composite ceramics.[25] In addition, it is noted that the $Q \times f$ value decreases promptly when $x \geq 0.3$, which is in accordance with the decrease in the relative density, because the pores in dielectric ceramics would degrade the $Q \times f$ values.[34–36] For the same reason, the increasing number of pores in ceramics with $x \geq 0.3$ would lead to an additional decrease in the $Q \times f$ values of the obtained $0.7Al_2Mo_3O_{12}$–$0.3TiO_2$ and $0.6Al_2Mo_3O_{12}$–$0.4TiO_2$ samples.

The temperature coefficients of the resonant frequencies (τ_f) of the obtained $(1-x)Al_2Mo_3O_{12}$–$xTiO_2$ ceramics are shown in Fig. 6 as a function of the x value. The obtained $Al_2Mo_3O_{12}$ ceramics without TiO_2 have a negative τ_f of −32.3 ppm °C^{-1}, which is a little higher than that of the reported pure $Al_2Mo_3O_{12}$ ceramics in ref. 22, possibly correlating with the increased density of the present sample. However, with x increasing from 0 to 0.4, the τ_f value rises up from −32.3 to +9.2 ppm °C^{-1}, during which the obtained $0.7Al_2Mo_3O_{12}$–$0.3TiO_2$ ceramic exhibited a near-zero τ_f value (−3.3 ppm °C^{-1}). This phenomenon can be explained as follows. In general, for two-phase microwave dielectric composite ceramics, the τ_f value is determined by the matrix and second phases in the samples, obeying the following mixing rule:

$$\tau_f = \nu_1\tau_{f1} + \nu_2\tau_{f2}, \quad (4)$$

where ν_1 and ν_2 represent the volume fractions of the components, and τ_{f1} and τ_{f2} are their τ_f values, respectively. For the present $(1-x)Al_2Mo_3O_{12}$–$xTiO_2$ (x = 0, 0.1, 0.2, 0.3, and 0.4) ceramics, the τ_f value of the $Al_2Mo_3O_{12}$ matrix is −32.3 ppm °C^{-1}, while that of the second phase TiO_2 is +460 ppm °C^{-1}.[24] After adding TiO_2, the τ_f value of the composite ceramics would be effectively adjusted from negative to positive.

In order to make the merits of the obtained $(1-x)Al_2Mo_3O_{12}$–$xTiO_2$ ceramics more clear, Table 1 compares the microwave dielectric properties of the present $0.7Al_2Mo_3O_{12}$–$0.3TiO_2$ ceramics with those of already-reported important Mo-based ceramics with near-zero τ_f values in the literature. It can be easily concluded that the present $0.7Al_2Mo_3O_{12}$–$0.3TiO_2$ composite ceramics have low ε_r values, high $Q \times f$ values, and near-zero τ_f values, and can be sintered at a low temperature of 790 °C, which would be very promising in LTCC applications.

Table 1 Microwave dielectric properties of several Mo-based ceramics with near-zero τ_f values

Composition	ε_r	$Q \times f$ (GHz)	τ_f (ppm °C^{-1})	Ref.
$0.8CaMoO_4$–$0.2TiO_2$	12.8	29 310	+10	24
$0.842ZnMoO_4$–$0.158TiO_2$	13.9	40 400	+2	26
$0.6BaMoO_4$–$0.4TiO_2$	13.8	40 500	−6.13	23
$0.7MgMoO_4$–$0.3TiO_2$	9.1	11 990	+3.2	25
$0.8BaMoO_4$–$0.2TiO_2$	12.8	29 310	+10	23
$0.7Al_2Mo_3O_{12}$–$0.3TiO_2$	6.23	51 630	−3.3	This work

4. Conclusions

$(1-x)Al_2Mo_3O_{12}$–$xTiO_2$ (x = 0, 0.1, 0.2, 0.3, and 0.4) ceramics were prepared by a conventional two-step solid-state reaction and sintering method. The effects of TiO_2 addition on the phase composition, microstructure, and microwave dielectric properties of the obtained ceramics were investigated. XRD and SEM analyses revealed that rutile TiO_2 could coexist with monoclinic $Al_2Mo_3O_{12}$ in the obtained samples. The microwave dielectric properties of the obtained ceramics have a close relationship with the amount of TiO_2 present. When the x value increases from 0 to 0.4, the ε_r value increases from 5.69 to 6.85, $Q \times f$ decreases from 73 910 to 45 720 GHz, and τ_f rises up from −32.3 to +9.2 ppm °C^{-1}. When x = 0.3, a temperature-stable microwave dielectric ceramic was obtained. The obtained $0.7Al_2Mo_3O_{12}$–$0.3TiO_2$ composite with ε_r = 6.23, $Q \times f$ = 51 630 GHz, and τ_f = −3.3 ppm °C^{-1} would be a very promising LTCC candidate for microwave wireless communications.

Conflicts of interest

There are no conflicts to declare.

Acknowledgements

This work was supported by the National Natural Science Foundation of China (grant no. 11674035 and 61274015), and the Fund of State Key Laboratory of Information Photonics and Optical Communications (Beijing University of Posts and Telecommunications).

References

1 M. T. Sebastian, R. Ubic and H. Jantunen, *Int. Mater. Rev.*, 2015, **60**, 392.
2 M. T. Sebastian and H. Jantunen, *Int. Mater. Rev.*, 2008, **53**, 57.

3 A. Sasidharanpillai, C. H. Kim, C. H. Lee, M. T. Sebastian and H. T. Kim, *ACS Sustainable Chem. Eng.*, 2018, **6**, 6849.
4 J. B. Lim, D. H. Kim, S. Nahm, J. H. Paik and H. J. Lee, *Mater. Res. Bull.*, 2006, **41**, 1199.
5 Y. Chen, E. Li, S. Duan and S. Zhang, *ACS Sustainable Chem. Eng.*, 2017, **5**, 10606.
6 S. O. Yoon, S. H. Shim, K. S. Kim, J. G. Park and S. Kim, *Ceram. Int.*, 2009, **35**, 1271.
7 H. Kagata, R. Saito and H. Katsumura, *J. Electroceram.*, 2004, **13**, 277.
8 C. F. Yang, Y. C. Chen, W. C. Tzou and S. L. Chang, *Mater. Lett.*, 2003, **57**, 2945.
9 D. Zhou, C. A. Randall, H. Wang, L. Pang and X. Yao, *J. Am. Ceram. Soc.*, 2010, **93**, 1096.
10 Y. Lee, J. Chiu and Y. H. Chen, *J. Am. Ceram. Soc.*, 2013, **96**, 1477.
11 A. Surjith and R. Ratheesh, *J. Alloys Compd.*, 2013, **550**, 169.
12 L. Pang, H. Liu, D. Zhou, G. Sun, W. Qin and W. Liu, *Mater. Lett.*, 2012, **72**, 128.
13 G. Choi, J. Kim, S. H. Yoon and K. S. Hong, *J. Eur. Ceram. Soc.*, 2007, **27**, 3063.
14 D. Zhou, H. Wang, X. Yao and L. Pang, *J. Am. Ceram. Soc.*, 2008, **91**, 3419.
15 G. Zhang, H. Wang, J. Guo, L. He, D. Wei and Q. Yuan, *J. Am. Ceram. Soc.*, 2015, **98**, 528.
16 L. Pang, G. Sun and D. Zhou, *Mater. Lett.*, 2011, **65**, 164.
17 A. R. Soares, P. I. Ponton, L. Mancic, J. R. M. D'Almeida, C. P. Romao, M. A. White and B. A. Marinkovic, *J. Mater. Sci.*, 2014, **49**, 7870.
18 R. Truitt, I. Hermes, A. Main, A. Sendecki and C. Lind, *Materials*, 2015, **8**, 700.
19 M. Ari, K. J. Miller, B. A. Marinkovic, P. M. Jardim, R. de Avillez, F. Rizzo and M. A. White, *J. Sol-Gel Sci. Technol.*, 2011, **58**, 121.
20 C. P. Romao, S. P. Donegan, J. W. Zwanziger and M. A. White, *Phys. Chem. Chem. Phys.*, 2016, **18**, 30652.
21 M. Wu, J. Peng, Y. Cheng, X. Xiao, D. Chen and Z. Hu, *J. Alloys Compd.*, 2013, **577**, 295.
22 A. Surjith, N. K. James and R. Ratheesh, *J. Alloys Compd.*, 2011, **509**, 9992.
23 J. Guo, D. Zhou, H. Wang, Y. Chen, Y. Zeng, F. Xiang, Y. Wu and X. Yao, *J. Am. Ceram. Soc.*, 2012, **95**, 232.
24 J. Guo, D. Zhou, L. Wang, H. Wang, T. Shao, Z. M. Qi and X. Yao, *Dalton Trans.*, 2013, **42**, 1483.
25 H. Zheng, S. Yu, L. Li, X. Lyu, Z. Sun and S. Chen, *J. Eur. Ceram. Soc.*, 2017, **37**, 4661.
26 J. Guo, D. Zhou, H. Wang and X. Yao, *J. Alloys Compd.*, 2011, **509**, 5863.
27 D. Di Marco, K. Drissi, P. M. Geffroy, N. Delhote, O. Tantot, S. Verdeyme and T. Chartier, *J. Eur. Ceram. Soc.*, 2017, **37**, 641.
28 A.-K. Axelsson, M. Sebastain and N. McNAlford, *J. Korean Ceram. Soc.*, 2013, **40**, 4.
29 H. J. Lee, I. T. Kim and K. S. Hong, *Jpn. J. Appl. Phys.*, 1997, **36**, L1318.
30 H. J. Lee, K. S. Hong, S. J. Kim and I. T. Kim, *Mater. Res. Bull.*, 1997, **32**, 847.
31 R. C. Pullar, J. D. Breeze and N. M. Alford, *J. Am. Ceram. Soc.*, 2005, **88**, 2466.
32 L. Li, H. Sun, X. Lv and S. Li, *Mater. Lett.*, 2015, **160**, 363.
33 Q. J. Mei, C. Y. Li, J. D. Guo and H. T. Wu, *Mater. Lett.*, 2015, **145**, 7.
34 M. He and H. W. Zhang, *J. Alloys Compd.*, 2014, **586**, 627.
35 G. Choi, S. Cho, J. Ana and K. Hong, *J. Eur. Ceram. Soc.*, 2016, **26**, 2011.
36 F. F. Gu, G. H. Chen, C. L. Yuan, C. R. Zhou and Y. Yang, *J. Mater. Sci.: Mater. Electron.*, 2015, **26**, 360.

